Title

Adaptive-optics optical coherence tomography for high-resolution and high-speed in vivo retinal imaging

Authors

Zawadzki, RJ
Choi, S
Laut, S
et al.

Publication Date

2005-12-19

Peer reviewed

Adaptive-optics optical coherence tomography for high-resolution and high-speed *in vivo* retinal imaging

Robert J. Zawadzki, Stacey Choi, Sophie Laut, and John S. Werner
Department of Ophthalmology and Vision Science, University of California Davis, 4860 Y Street, Suite 2400, Sacramento, California 95817
rjzawadzki@ucdavis.edu

Steven M. Jones and Scot S. Olivier
Lawrence Livermore National Laboratory, 700 East Avenue, Livermore, California 74550

Mingtao Zhao, Bradley A. Bower and Joseph A. Izatt
Department of Biomedical Engineering, Duke University, 101 Science Drive, Durham, North Carolina 27708

Abstract: We have combined Fourier-domain optical coherence tomography (OCT) with a closed-loop Adaptive Optics (AO) system. The AO-OCT instrument has been used for *in vivo* retinal imaging. High-lateral resolution of our AO-OCT system allows visualization of the microscopic retinal structures not accessible by standard OCT instruments.

OCIS codes: (110.4500) Optical coherence tomography; (010.1080) Adaptive optics

1. Introduction

Time-domain optical coherence tomography (OCT) [1] has, within only about a decade, become widely incorporated into clinical research and practice in ophthalmology. A significant advance in OCT within the last few years has been made possible by Fourier-domain OCT [2]. This method permits measurements at a much higher speed and with higher sensitivity than standard time-domain OCT [3-5]. Several groups have also reported Fourier-domain OCT systems for *in vivo* real-time imaging at ultrahigh resolution (UHR) as well as with Doppler, and polarization-sensitive OCT. Due to the high speed of Fourier-domain OCT, the 3D imaging of *in vivo* retinal structures has been possible as well. Axial resolution with these methods has been improved to a few μm due to the development of novel light sources. Transverse resolution in this domain has generally remained at 15 to 20 μm.

The first attempt to improve transverse resolution with adaptive optics has been reported by Miller et. al [6] for *en face* coherence gated OCT and by Hermann et. al [7] for UHR-OCT. Both of these groups used adaptive optics technology with a Hartmann-Shack wavefront sensor and a deformable mirror operating in a closed loop. Miller et al [8] have recently described the use of AO line-illumination parallel Fourier Domain OCT allowing photoreceptor imagining on single B-scans. Improvements in transverse resolution sufficient to image the photoreceptor mosaic have also been realized with adaptive optics in flood-illumination imaging and the scanning laser ophthalmoscope [9-10], but axial resolution is lower than that expected from OCT.

In this paper we describe a hybrid AO-OCT instrument combining for the first time, to our knowledge, the advantages of standard confocal Fourier-domain OCT and the latest technology for adaptive optics. By correcting ocular aberrations with AO, the scanning beam diameter is reduced on the retina while maintaining the same axial resolution and high speed characteristic of scanning Fourier-domain OCT. The resultant axial and transverse resolution of AO-OCT exceeds that which is possible for AO or OCT alone. The first images acquired with this system show the great potential of this novel instrument.

2. Materials and methods

The AO-OCT system presented in this paper occupies 1 m x 1 m of a standard laboratory optical table. The sample arm utilizes a Hartmann-Shack wavefront sensor and a 37-electrode bimorph deformable mirror for aberration correction. The same light has been use for OCT as well as Hartmann-Shack detection channels. Two independent PCs have been used, one for AO control and one for the OCT scanning and detection unit. A bite bar, forehead-rest and fixation target are used to minimize head and eye motion. The subjectís eye is also dilated and cyclopleged with drops (Tropicamide & Cyclogel) allowing imaging over 7mm pupil diameter.

Optical Coherence Tomography and Coherence Techniques II, edited by Wolfgang Drexler,
Proc. of SPIE-OSA Biomedical Optics, SPIE Vol. 5861 © 2005 SPIE and OSA · 1605-7422/05/$15

2.1 Theory

In our Fourier-domain OCT system [11] a spectrometer is used to measure the spectrum of the light that returns from the reference and sample arms. Depth information (equivalent to an A-scan in the time-domain) is accessed by the inverse FTT of the spectrometer signal. To improve image quality we used DC subtraction, λ to k transformation (including dispersion compensation, interpolation) and zero padding methods already described by other groups. To overcome the problem of the complex conjugate image after Inverse Fourier Transform we placed our reference mirror such that the zero path length difference is negative for the whole retinal structure.

The control of the deformable mirror for AO requires the use of the classical singular value decomposition (SVD) method, already well-described in the literature [12], to generate the set of voltages associated with the reconstruction of a specific wavefront. In brief, the wavefront is measured in terms of centroid displacements from the Hartmann-Shack wavefront sensor (i.e., the association of a lenslet array and a CCD camera placed in its focal plane). The influence functions of the deformable mirror (i.e., the individual responses of each actuator when the others are set to zero) are first recorded and stored into a so-called î influence matrix.î To control the set of voltages to be applied to the electrodes of the mirror to achieve a specific wavefront (or specific centroid displacements), the matrix must be inverted. This matrix is, however, not square and requires decomposition with the SVD method into the product of 3 matrices, one among them being diagonal, in order to be inverted in a second step.

2.2 Experimental

The experimental setup is shown in Figure 1. The heart of the OCT system is a fiber-based Michelson interferometer. The source was a superluminescent diode (SLD) from Superlum (λ_O = 841 nm, $\Delta\lambda$ = 50 nm, P = 9 mW), with measured axial resolution of Δz = 6 μm in free space.

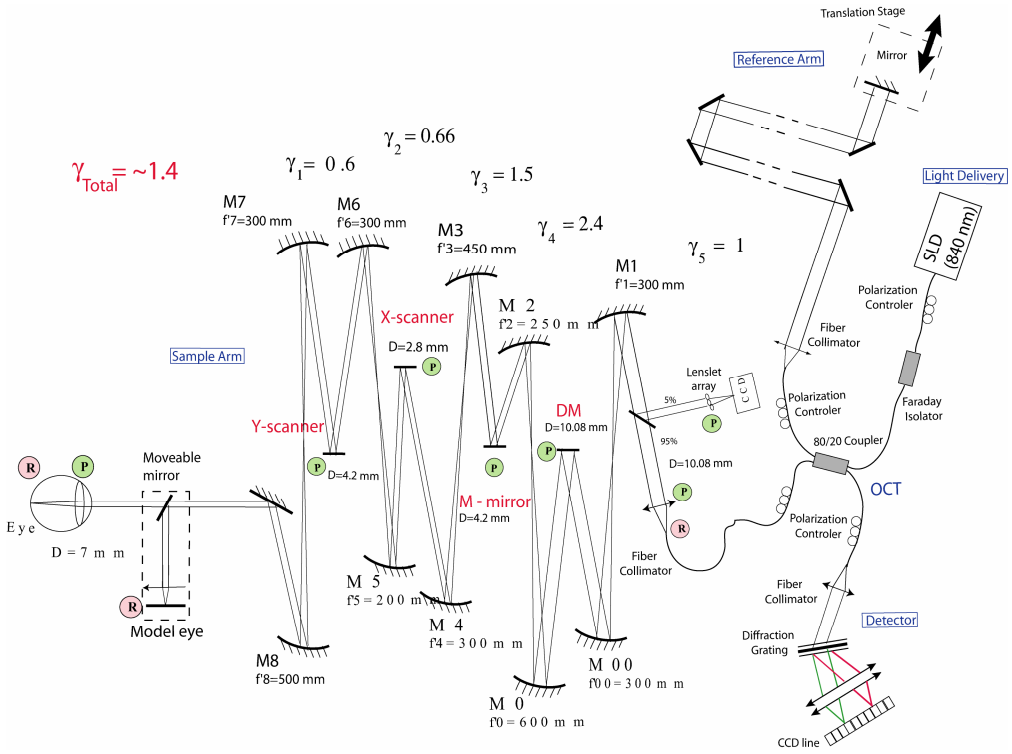

Fig. 1. Schematic of experimental setup. The reference arm length has been shortened in this illustration to simplify the image. γ - magnification, D- diameter, f ñ focal length, DM ñ Deformable Mirror, M ñ mirror, P ñ conjugated pupil planes, R ñ conjugated retinal planes.

A fiber-based Faraday isolator (OZ optics) protects the SLD against back reflections. The 80/20 fiber coupler (AC photonics) splits light into the reference and sample arms. The translation stage in the reference arm is used to match the path length in both interferometric arms. We used a water vial to initially compensate the dispersion of the

human eye. An OCT-PC drives the two x- and y-galvo scanners allowing different scanning modes, standard B-scans, radial, circular as well as 3D acquisition. The detected OCT signal is post-processed and displayed in real time, and then saved in the PCís RAM memory. The detection spectrometer uses a CCD line-scan camera (12 bit, Atmel, 2048-pixels). The light in the spectrometer is collimated using a 100 mm focal length collimating objective (OZ optics) in front of the 1200 l/mm holographic transmitting diffraction grating (Wasatch Photonics). Two 300 mm focal length doublets are used to focus the light onto the CCD. The current system data acquisition speed equals 9,000 A-scan for 100 µs exposure and 18,000 A-scans for 50 µs exposure. The standard system setting allows frame rates varying from 9 Frames/s (1000 A-scans / Frame; 100 µs exposure) to 36 Frames/s (500 A-scans / Frame; 50 µs exposure) After finishing acquisition, depending on our settings, the last 100 or 200 Frames are streamed to the PCís hard drive. With the current spectrometer design the maximum axial range (seen after Fourier Transform) is 2.7 mm in free space and approximately 2 mm in the eye. The power at the subjectís eye is equal to 400 µW. The same OCT engine has also been used for standard clinical imaging proving its performance and reliability.

As already noted, to achieve improved transversal resolution the sample arm has been modified to incorporate an AO unit to monitor and correct wavefront aberration of the imaged eye. Our design uses spherical mirrors instead of lenses commonly used in OCT to reduce dispersion matching problems as well as back reflections that can occur while the scanners are moving. The optical design of the sample arm ensures that the exit pupil of the eye is conjugate with the x and y scanning mirrors (which limits scanner motion error observed on the wavefront sensor) as well as with the bimorph deformable mirror and the Hartmann-Shack wavefront sensor. This is achieved by using pairs of spherical mirrors working as imaging telescopes. An extra conjugated pupil plane with a flat mirror is left for future incorporation of a Micro Electro Mechanical (MEMS) deformable mirror. The AO-control computer reads the data from the wavefront sensor (Dalsa 1M60 CCD camera and 20x20 lenslet array) and sends commands to the AOptix Bimorph deformable mirror. The wavefront sensor operates at 25 Hz; the global control loop performs the correction of the aberrations with the same temporal frequency.

3. Results

The performance of our stand-alone OCT system (with standard ìshorterî sample arm) was tested for retinal imaging prior to incorporating the AO system. The figure below shows the resultant high-resolution image (Δz = 3,6 µm) acquired over 6mm range on a fovea. We also present here our labeling of retinal layers based primarily upon light microscopy [13].

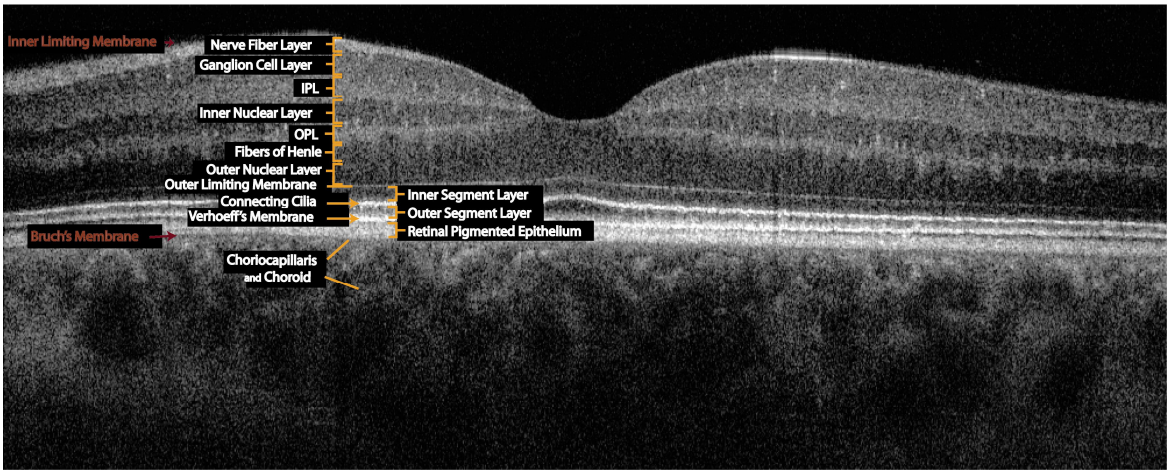

Fig. 2. High-resolution B-scan of retinal structures acquired with our OCT instrument (4000 A-scans) We have identified the following retinal layers known from the literature: Nerve Fiber Layer (NFL), Ganglion Cell Layer (GCL), Inner Plexiform Layer (IPL), Inner Nuclear Layer (INL), Outer Plexiform Layer (OPL), Fibers of Henle, Outer Nuclear Layer (ONL), Inner Segment Layer (ISL), Outher Segment Layer (OSL), Retinal Pigment Epithelium(RPE), Choriocapillaris and Choroid. The Outer Limiting Membrane (sometimes called External Limiting Membrane), Connective Cilia and Verhoeffis Membrane may also be seen. The Inner Limiting Membrane and Bruchís Membrain are not visible on this image but its position has been confirmed using the same OCT system for imaging diseased retinas.

Next, the same OCT engine was incorporated into our AO-OCT scanning instrument to allow improved lateral resolution. We also changed the light source used in our AO-OCT instrument to another Superluminescent diode with a longer coherence length.

To test the AO-system performance we imaged a model eye with a business card used as a retina. Different sets of trial lenses have been placed in a front of it to test the system performance. We found out that our DM can correct up to +/- 4 Diopter (D) defocus and +/- 1 D cylinder. As an example, the 3D structure of the front side of the business card with AO turned ON and OFF is shown in Fig. 3. These images have been created using a set of 100 Frames with 1000 A-scans / Frame.

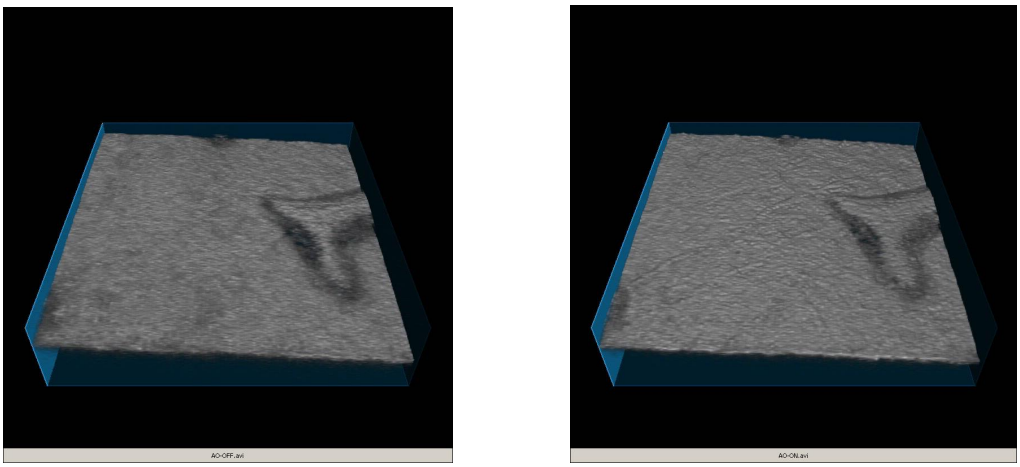

Fig. 3. 3D reconstruction of the business card with 0.25 D defocus and 0.25 D cylinder trial lenses, uncorrected (left) and corrected (right).

As can be seen, an improvement of the lateral resolution after turning AO on results in increased image intensity as well as better visualization of paper texture. This has been achieved due to a tenfold reduction of the RMS wavefront error.

Next, a healthy 30 year-old volunteer was tested to produce AO-corrected Fourier-domain OCT images. Fig. 4 shows the change in image quality with real time values of RMS error recorded during measurements.

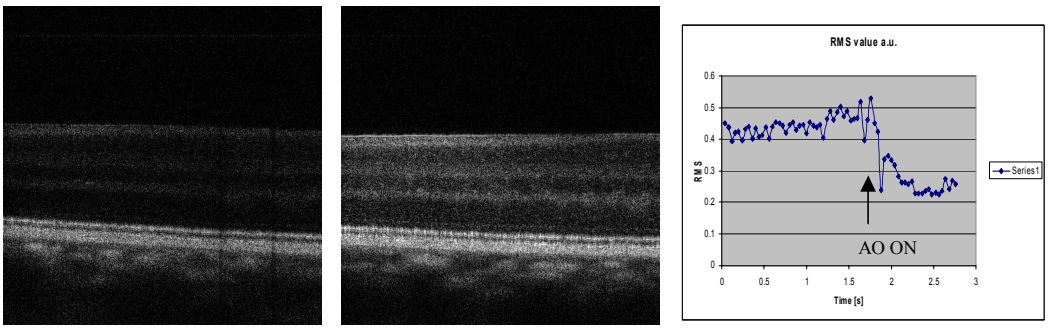

Fig. 4. Left and center images show human retina without and with AO imaged for person with emmetropic eye respectively. The image covers 1x1mm (1000 A-scans / Frame). The right panel show a typical RMS error graph as a function of time during start of AO correction (starting point of AO control is marked by arrow).

A clear improvement in image brightness as well as better visualization of retinal structures can be observed with AO. Because of the large pupil size used in our system, the theoretical depth of focus and thus the useful range of best lateral resolution is limited to about 100 µm. To further demonstrate the improved image resolution with AO, we have developed a method for controlling our DM by introducing arbitrary amounts of defocus while still correcting the remaining aberrations. This allows systematic shifts in the axial position of the imaged beam focus. We used seven different settings of the DM creating the following defocus in the imaged eyeís pupil plane (1.5 D, 1 D,

0.5 D, 0 D, - 0.5 D, - 1 D and - 1.5 D) to demonstrate the increase of the structure intensity due to better coupling of imaged structure. Figure 5 shows the B-Scans with associated intensity profiles for all seven DM defocus values.

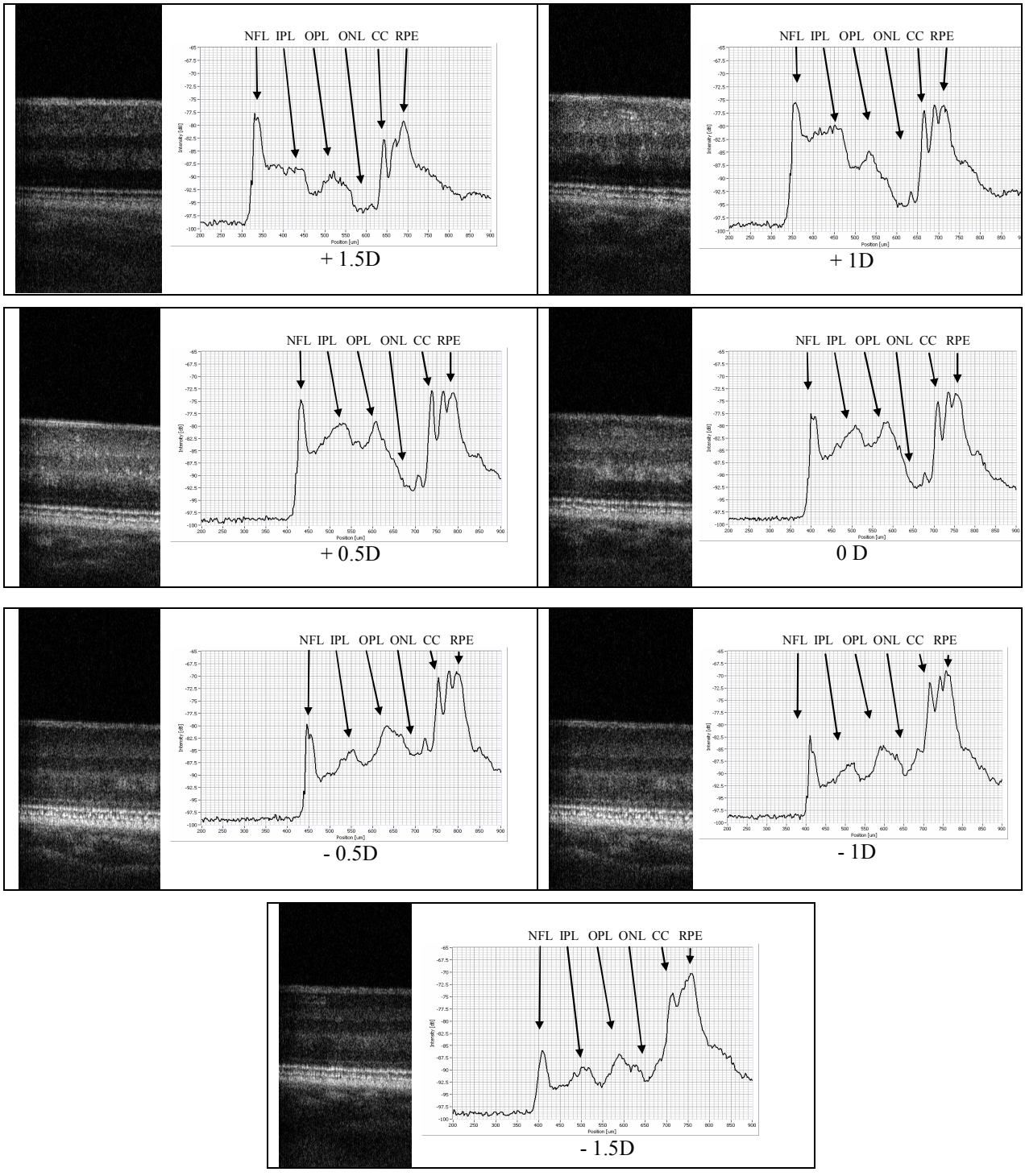

Fig. 5. *In vivo* OCT images of AO corrected retinal structures with intensity axial profiles for seven different focusing positions. The narrow depth of focus manifests itself by increases in intensity of the structures at the beam focus. All images have been acquired over 500 μm lateral distance.

As can be seen from the results above, in order to fully use the advantages of increased transversal resolution of an AO-OCT system the observed structure must lay inside the depth of focus. We also found out that standard B-scan representations of OCT images do not fully illustrate the improved resolution of AO-OCT. For this reason, we have examined C-scans reconstructed from 3D volume rendering of B-scans. For all C-scan images presented in this paper, the focus was placed inside a specific retinal layer. In order to have relatively dense sampling in the lateral plane and at the same time to reduce the 3D data acquisition time, and therefore the eye motion artifact, most of our images have been acquired in 200x500 (A-scans / Frame) mode. Thus the time needed to acquire the whole 3D structure (for 50 µs exposure time) was equal to 5.5s. The images have been acquired over 0,5 to 1mm rectangular area on the retina, which results in 1 to 2 µm sampling density. Before 3D reconstruction all frames have been registered in a semi automatic way for axial eye motion. No post processing has been used to reduce blur associated with lateral eye motion.

Figures 7, 8, 9 10 and 11 show C-scans (lateral planes) cut from the 3D data sets in the plan of the nerve fiber layer, ganglion cell layer, inner nuclear layer, connecting cilia (between the inner and outer segments of photoreceptors) and retinal pigmented epithelium. The cutting plane orientation is schematically presented on the figure below:

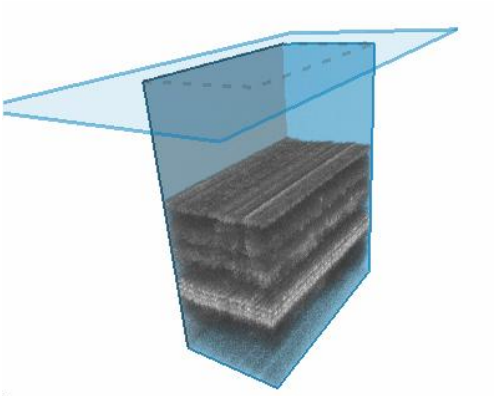

Fig. 6. C-scan cutting plane orientation superimposed on 3D visualisation of retina structure.

All the B-scans images presented below cover 500 µm (1,5 deg) x 1mm (lateral x axial) area. Each figure caption presents further information about C-scan location as well as its size and sampling density.

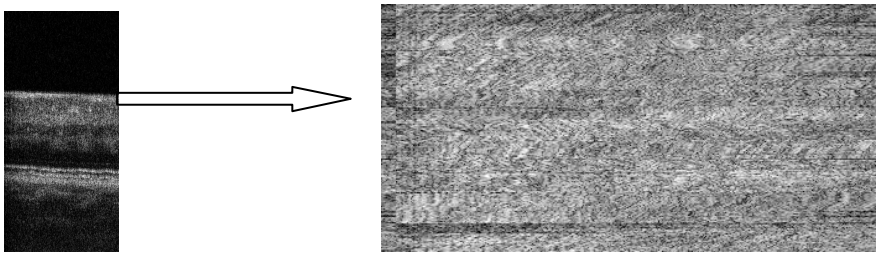

Fig. 7. Nerve Fiber Layer structure as seen with DM defocus value of + 1D. C-scan image size: 200x400µm (0,6 x1,2 deg) (lateral sampling 1 µm), eccentricity of 4 deg temporal retina (TR)

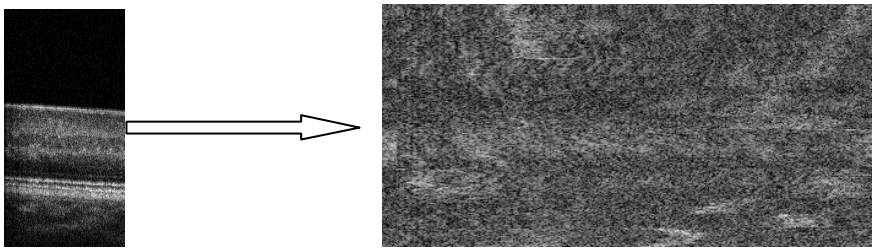

Fig. 8. Ganglion Cell Layer structure as seen with DM defocus value of + 0.5D. C-scan image size: 200x400µm (0,6 x1,2 deg) (lateral sampling 1 µm), eccentricity of 4 deg TR

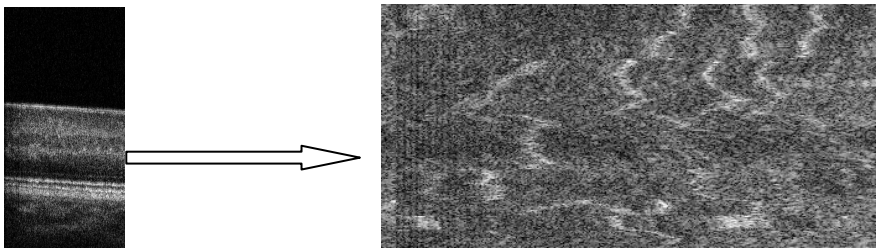

Fig. 9. Micro-vasculature in Inner Nuclear Layer as seen with DM defocus value of + 0.5D. C-scan image size: 200x400μm (0,6 x1,2 deg) (lateral sampling 1 μm), eccentricity of 4 deg TR

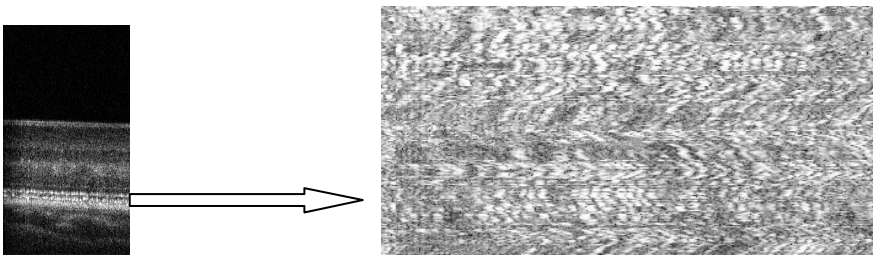

Fig. 10. Connecting Cilia (between inner and outer segments of the photoreceptors) as seen with DM defocus value of ñ 0.5D. C-scan image size: 200x400μm (0,6 x1,2 deg) (lateral sampling 1 μm), eccentricity of 4 deg TR

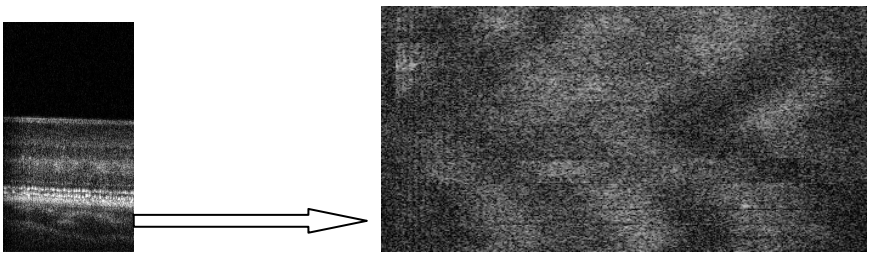

Fig. 11. Choroidal structures as seen with DM defocus value of ñ 0.5D. C-scan image size: 200x400μm (0,6 x1,2 deg) (lateral sampling 1 μm), eccentricity of 4 deg TR.

4. Conclusions

The performance of the AO-OCT system presented in this paper is similar to that described by others using time-domain as well as line illumination Fourier-domain AO-OCT. That is, there is an increase in the system sensitivity (manifested as change in image brightness). Moreover, high acquisition speed allows for the first time the 3D data collection and further C-Scan image evaluation, important for the comparison of AO-OCT system performance with other imaging instruments (e.g., flood- illumination AO and AO-SLO). Initial testing demonstrates excellent correction of large optical aberrations using the bimorph DM, but an additional DM may be necessary to better correct the higher-order aberrations.

As can be seen on all reconstructed C-scans, due to the nature of our imaging technique (it is the relatively slow scanning speed if compared to transversal OCT) the lateral motion of the eye introduces strong distortion and blurring of the imaged structure. However, one of the main advantages of this approach is relatively simple implementation of axial eye motion correction, allowing visualization of thin retina layers and intersections.

The introduction of a pupil camera should improve the AO system performance due to more precise alignment of the entrance pupil plane of the system, thereby improving image quality. Further design changes are being implemented to exploit the full advantage expected from incorporating AO with OCT.

Acknowledgements

We gratefully acknowledge the contributions of Donald T. Miller, Jungtea Rha and Yan Zhang from the School of Optometry, Indiana University, Bloomington. This research was supported by the National Eye Institute (grant EY 014743).

References

1. D. Huang, E. A. Swanson, C.P. lin, J.S. Schuman, W.G. Stinson, W. Chang, M.R. Flotte, K. Gregory, C.A. Puliafito, ì Optical Coherence Tomographyî , Science **254**, 1178-1181 (1991)
2. A. F. Fercher, C.K. Hitzenberger, G. Kamp, Y. Elzaiat, ì Measurement of intraocular distances by backscattering spectral interferometryì , Opt. Commun. **117**, 43-48 (1995)
3. M. Wojtkowski, T. Bajraszewski, P. Targowski and A. Kowalczyk, ì Real time in vivo imaging by high-speed spectral optical coherence tomographyî , Opt. Lett. **28**, 1745-1747 (2003)
4. R. Leitgeb, C.K. Hitzenberger, and A.F. Fercher ì Performance of fourier domain vs. time domain optical coherence tomographyî , Opt. Express **11**, 889-894 (2003)
5. N.A. Nassif, B. Cense, B.H. Park, M.C. Pierce, S.H. Yun, B.E. Bouma, G.J. Tearney, T.C. Chen, J,F. de Boer ì In vivo high-resolution video-rate spectral-domain optical coherence tomography of the human retina and optic nerveî , Opt. Express **12**, 367-376 (2004)
6. D.T. Millller, J. Qu, R.S. Jonnal, and K. Thorn, ì Coherence gating and adaptive optics in the eyeî in Coherence Domain Optical Methods and Optical Coherence Tomography in Biomedicine VII, Valery V. Tuchin, Joseph A. Izatt, James G. Fujimoto, Proc. SPIE 4956, 65-72 (2003)
7. B. Hermann, E.J. Fernandez, A. Unterhubner, H. Sattmann, A.F. Fercher, and W. Drexler, P.M. Prieto and P. Artal, ì Adaptive-optics ultrahigh-resolution optical coherence tomographyì , Opt. Lett. **29**, 2142-2144 (2004)
8. Y. Zhang, J. Rha, R.S. Jonnal, D.T. Miller, ì Adaptive optics parallel spectral domain optical coherence tomography for imaging the living retina,î Opt. Express (in press).
9. J. Liang, D.R. Williams and D.T. Miller, ì Supernormal vision and high-resolution retinal imaging through adaptive optics ì , J. Opt. Soc. Am. A 14, 2884 (1997)
10. A. Roorda, F. Romero-Borja, W.J. Donnelly III, H. Queener, T.J. Hebert, and M.C.W. Campbell, ì Adaptive optics scanning laser ophthalmoscopy ì , Opt. Express 10, 405-412 (2002)
11. R.J. Zawadzki, B.A. Bower, M. Zhao, M. Sarunic, S. Laut, J.S. Werner and J.A. Izatt, ì Exposure time dependence of image quality in high-speed retinal *in vivo* Fourier-domain OCT,î in Ophthalmic Technologies XV; Fabrice Manns, Per G. Soederberg, Arthur Ho, Bruce E. Stuck, Michael Belkin; Proc. SPIE**,** 5688, 45-52 (2005)
12. R.K. Tyson, *Principle of Adaptive Optics* (Academic Press, inc., 1991), Chap. 7.
13. R.W. Rodieck, *The Vertebrate Retina*, (W.H. Freeman, San Francisco, 1973).